Submarine landslides along the Siberian termination of the Lomonosov Ridge, Arctic Ocean

Ursula Schlager [a,*], Wilfried Jokat [a,b], Estella Weigelt [a], Catalina Gebhardt [a]

[a] Alfred Wegener Institute Helmholtz Centre for Polar and Marine Research, Am Alten Hafen 26, Bremerhaven 27568, Germany
[b] University of Bremen, Geoscience Department, Klagenfurter Str. 4, 28359 Bremen, Germany

ARTICLE INFO

ABSTRACT

Acoustic and detailed swath bathymetry data revealed a systematic picture of submarine landslides on the Siberian part of Lomonosov Ridge. Whereas numerous studies on mass movement exist along the margin of the Arctic Ocean less is known from central Arctic. A regional survey comprising swath bathymetry, sediment echo sounder and multichannel seismic profiling was performed on the southeastern Lomonosov Ridge. The data provide constraints on the present-day morphology of the Siberian part of Lomonosov Ridge, between 81°–84°N and 140°–146°E. We mapped twelve crescent-shaped escarpments located on both flanks on the crest of Lomonosov Ridge. The escarpments are 2.1 to 10.2 km wide, 1.7 to 8.2 km long and 125 to 851 m high from which 58 to 207 m are occupied by crescent-shaped headscarps. Subbottom data show chaotic reflections within most of the escarpment areas. The unit is overlain by ~110–340 m of semi-coherent parallel reflections. At its bottom the chaotic reflections are limited by a partly eroded high-amplitude reflection sequence that is inclined with <1° basinwards. We find the escarpments to be remnants of submarine landslide events that mobilized 0.09 to 7.58 km^3 of sediments between mid Pliocene and mid Miocene. The relatively small amounts of mobilized sediments seem to be typical for the Lomonosov Ridge. The epoch corresponds to the ongoing subsidence of the Lomonosov Ridge below sea level. During that time deposition and the load of sediments changed. We suggest that changes in sediment type preconditioned, and co-occurring earthquakes finally triggered the submarine landslides.

© 2021 Published by Elsevier B.V.

1. Introduction

Submarine landslides are known from continental margins worldwide. They occur on all types of margins and vary tremendously in size (e.g. Canals et al., 2004; Masson et al., 2006; Mosher et al., 2010). The largest currently-known surficial landslide, the Holocene Storegga Slide (2400–3200 km^3, Haflidason et al., 2004, 2005), is located off the Mid-Norway margin (Haflidason et al., 2004). Several studies refer to it as "Storegga slides" (Vogt et al., 1999) or "slide complex" (Bryn et al., 2003) since it is the result of a succession of events (Bugge et al., 1987, 1988). Numerous smaller submarine landslides are found north of Storegga, for instance on the eastern flank of the Jan Mayen Ridge (Laberg et al., 2014), in the Fram Strait west of Svalbard (Freire et al., 2014), and along the Northwest Barents Sea continental margin (Safronova et al., 2017). The northernmost mapped mass wasting event is the Hinlopen/Yermak Slide (Vanneste et al., 2006, Winkelmann et al., 2006) off Hinlopen Strait, on part of the North Svalbard continental margin. Difficult sea ice conditions have, however,

inhibited the acquisition of systematic swath bathymetric data from the central Arctic Ocean to get a complete overview on such features in the Arctic. However, some escarpments indicating submarine landsliding were reported e.g. from Canada Basin (Mosher et al., 2012), the Alpha Ridge (Boggild et al., 2020, Kristoffersen et al., 2008) and from Lomonosov Ridge in an area close to the North Pole (Kristoffersen et al., 2007).

Submarine landslides are an integral part of passive rifted continental margins around the world. The Lomonosov Ridge is a continental sliver (Jokat et al., 1992, Karasik, 1968) in the center of the Arctic Ocean resulting first from opening of Amerasia Basin, when the ridge was still part of the Siberian margin. Then, during the Cenozoic, the rifting and subsequent sea floor spreading detached the ridge from the Eurasian continent. Consequently, both flanks of the ridge represent rifted margins. Such double-sided rifted margin is unique in a global context, while the remaining vast majority of rifted margins underwent only a single rifting event. The only analogue to Lomonosov Ridge can be found at the west coast of Mexico. The difference to the Arctic is that the Baja California peninsula is currently still subaerially attached to the North American continent. Here, the analogue to the Eurasia Basin is the Gulf of California off western Mexico.

* Corresponding author.
E-mail address: Ursula.Schlager@awi.de (U. Schlager).

Topographically, Lomonosov Ridge rises several kilometers above the adjacent abyssal plains (Jakobsson et al., 2012) (Fig. 1a). Due to its pronounced topography the ridge influences ocean current systems (Weigelt et al., 2020, Woodgate et al., 2001), and was subject to glaciogenic processes (e.g. Jakobsson et al., 2016, Stein et al., 2016). The flanks of the ridge are sediment starved because there is no extensive hinterland. This makes the Lomonosov Ridge unique in comparison to most rifted margins. In northern hemisphere north of 80°N the sedimentary environment for Lomonosov Ridge is only comparable with other polar submarine plateaux or ridges (e.g. Alpha-Mendeleev Ridge) within the Central Arctic Ocean. In contrast, glaciated margins in the south (e.g. East Greenland, Arndt et al., 2017) or surrounding the Central Arctic Ocean are strongly modified by glaciers and ice streams with large onshore catchment areas. This is missing on Lomonosov Ridge. After its subsidence below sea level the ridge faced only current controlled erosion if

any. During glacial times its crest has been partly modified by deep reaching ice bergs (Jakobsson et al., 2016, Stein et al., 2016), and sediments delivered by the sea ice cover/ice floes (Dowdeswell et al., 1998, Nürnberg et al., 1994). Sediments transported on the subaerial ice surface and released by melting or floe fragmentation, is here the controlling process.

This study presents a part of the eastern Lomonosov Ridge close to the Laptev Sea margin to show the distribution of submarine landslides on the rims of the ridge and how they contribute to its present-day morphology.

2. Methods and data

Swath bathymetry, sediment echo sounder and seismic reflection data presented in this study were collected during mostly ice-free conditions with RV *Polarstern* in September 2014 (Stein, 2015).
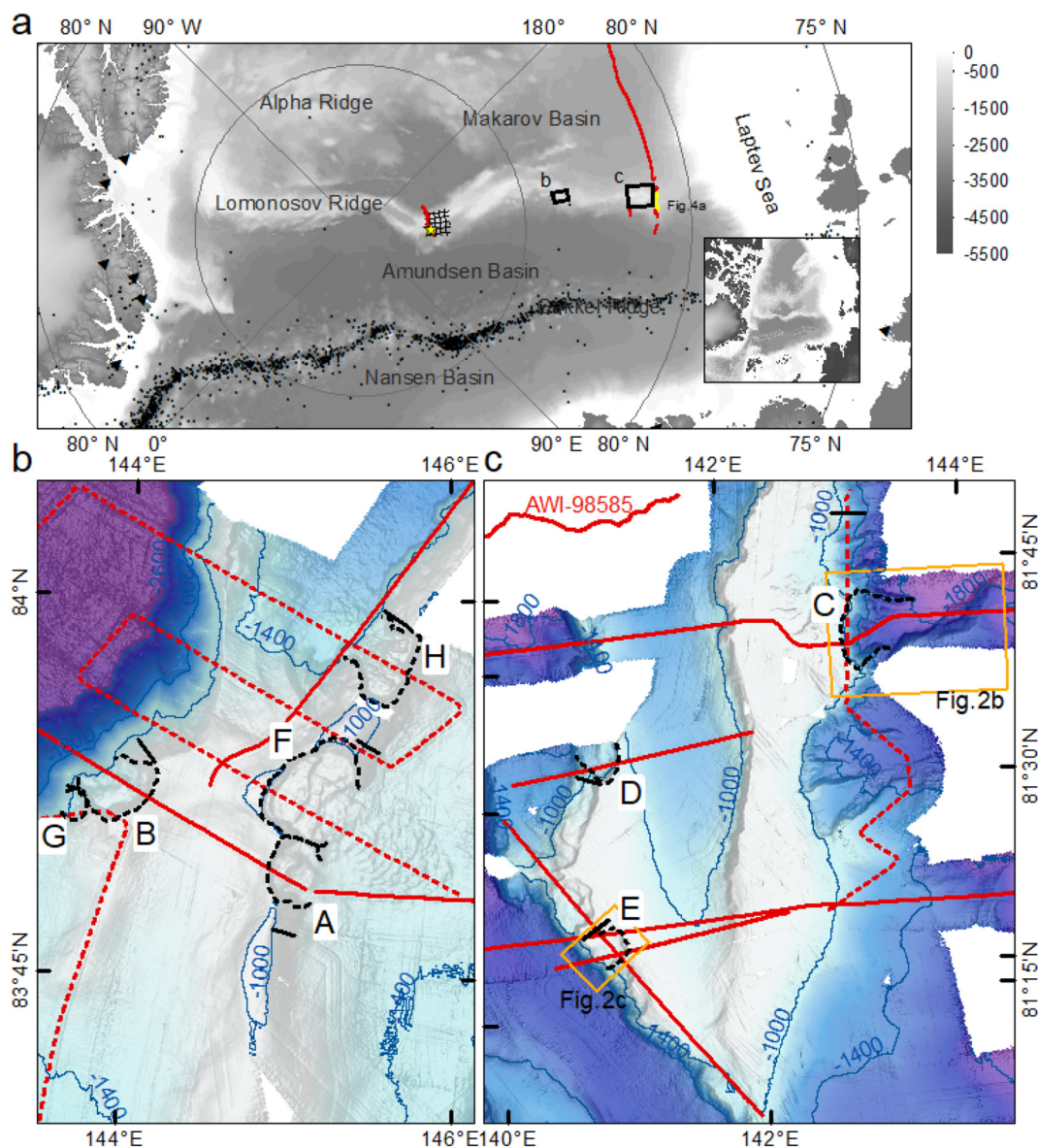

Fig. 1. Overview map and research area: (a) International Bathymetric Chart of the Arctic Ocean (IBCAO) (Jakobsson et al., 2012). Solid red lines (north to south): seismic reflection profiles AWI-91090 (Jokat et al., 1992, 1995), AWI-98585 (Jokat, 2005) and 81°N-Transect (Jokat et al., 2013), yellow star: ACEX-drilling site, yellow line on 81°N-Transect: seismic reflection profile part shown in Fig. 5, black dots and triangles: locations of detected earthquakes and seismometers, respectively, over the last 50 years (International Seismological Centre, 2020), hatched area: study area of submarine landslides of Kristoffersen et al. (2007); (b) and (c) new swath bathymetry data from 2014 separated in northern (b) and southern (c) research area. Both areas reveal crescent-shaped headscarps. Dashed black lines: top of headscarps A to H studied in this paper, solid straight black lines: sections for slope measurements, solid red lines: seismic reflection and sediment echo sounder profiles, dashed red lines: solely sediment echo sounder profiles.

In total, 10,371 km of swath bathymetry profiles were collected covering an area of 80,935 km^2 (Stein, 2015). The data were obtained with the ATLAS Hydrographic Hydrosweep DS3 multibeam echo sounder, which is permanently mounted on RV *Polarstern*. Within the research area, the swath width was set to 4–5 times the water depth with a vertical resolution of ~0.5% of the water depth, i.e. 5 m vertical resolution at a depth of 1000 m (Stein, 2015). Expendable conductivity-temperature-depth measurements were collected for sound velocity correction to calibrate the depth calculations of the swath data (Stein, 2015). The data were processed using CARIS HIPS & SIPS software. They were corrected for reflection errors, cleaned from coarse depth errors and, subsequently, gridded with a cell size 30 × 30 m.

Subbottom profiling data were obtained with a hull-mounted deep sea sediment echo sounder ATLAS Hydrographic PARASOUND DS III-P70 on RV *Polarstern*. The following settings were applied: primary frequencies of 20 and 24 kHz resulting in a secondary low frequency (SLF) of 4 kHz, pulse length of 0.5 ms and a beam angle of 4°. SLF data were recorded in ASD and PS3 format, converted to standard SGY format and, finally, imported into IHS Kingdom for further visualization and interpretation.

Due to variable ice conditions two different hydrophone streamers were used for the multichannel seismic (MCS) data acquisition. While operating in close sea ice, a 300-m-long analogue Prakla streamer with 48 channels (group interval of 6.25 m) and an air gun array of 6 G-guns (fired every 15 s, shot point spacing ~40 m) were operated. The recording length was 12 s with a sample rate of 2 ms. A total of 287 km of seismic data were acquired with this setup. In areas with little or no sea ice, a 3000 m digital Sercel Sentinel solid streamer with 240 channels (group interval of 12.50 m) together with an air gun array of 3 G-guns (fired every 15 s, shot point spacing ~40 m) was used, acquiring a total of 2058 km of data. The recording length was 12 s with a sample rate of 1 ms.

The seismic data processing comprised common depth point sorting with 25 m bin spacing, band pass filtering, velocity analysis, spherical divergence and normal moveout correction, and stacking as well as post-stack time migration.

We used swath bathymetry data to measure the spatial extent and to calculate the volumes of material missing on the seafloor as indicated by scars on the seafloor topography. For the latter, we estimated the sediments that are missing on the surface by calculating the difference between the present seafloor topography and a hypothetical pre-surface that connects the upper scar edges (Canals et al., 2004, Clare et al., 2019). The pre-surface was calculated with the method spline with barriers (Zoraster, 2003).

We measured the gradients of such scars via analysis of the inclination values of all bathymetric grid points related to the scar. The result is presented as box plot displaying the minimum and maximum value, first and third quantile as well as median and mean values of this analysis (Fig. 2). This method seems us more reliable than measuring
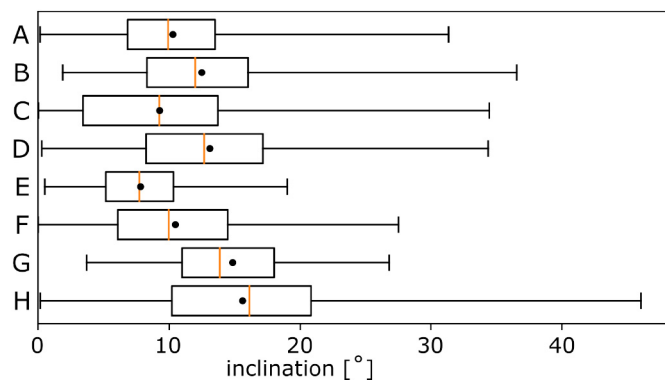

Fig. 2. Inclination values for headwalls: plotted as boxplot showing, from left to right: minimum, first quantile (start of box), median (orange, vertical line in box), mean (dot), third quantile (end of box), maximum inclination value.

the inclination of an along-slope line, which is unlikely to be representative of the variability of the scar. Normal gradients, however, were measured using along-slope lines in undisturbed areas next to each scar (Fig. 1b, c).

MCS and sediment echo sounder profiles are used to calculate the volume of subbottom sediments. We applied a seismic velocity of 1.7 km/s for depths and dip calculations of the shallow sediments.

3. Results

Swath bathymetry data reveal twelve transverse escarpments between 81° and 84°N and 140° and 146°E, located on both sides of the crest of the Lomonosov Ridge and oriented to the adjacent basins. These features cover roughly 7% of the investigated research area. Eight of them are investigated in greater detail (Fig. 1b, c: A-H). The escarpments typically comprise a steep, up to ~21° (3rd quantile, Fig. 2) inclined, crescent-shaped headscarp that borders a lower level area. The surrounding topography is basinwards inclined with slopes of up to 14°. The escarpments are 2.1–10.2 km wide and 1.7–8.2 km long. Their total height ranges from 125 to 851 m from which 58–207 m are occupied by the headscarp. And the volumes missing in each escarpment span over two orders of magnitude from 0.09 to 7.58 km^3 (Table 1).

MCS and sediment echosounder data are available for a few of the newly discovered escarpments. They cross them randomly because the expedition was originally not targeted to map escarpments on the ridge. Where available, seismic data show that the seafloor in the escarpment region is covered by 130 ms to 400 ms TWT (~110–340 m) of semi-coherent parallel subbottom reflections interbedded with acoustically transparent lens-shaped deposits (Fig. 3d). Outside the escarpment region i.e., on the crest of the ridge, the upper semi-coherent reflections continue with lower amplitude and overly conformably a high-amplitude reflection sequence (HARS). Hence, the upper sequence reaches thicknesses of ~550 ms TWT (~470 m) in the northern research area and, on average, 630 ms TWT (~540 m) in the southern research area. Inside the escarpment region, a chaotic subbottom reflection is observed between the semi-coherent unit on top and the HARS below (Fig. 3c). Here, the HARS dips towards the adjacent basins with less than 1° and, furthermore, it shows traces of erosion at its interface to the chaotic unit. The chaotic unit is confined to the escarpment area (Fig. 3c). Calculations of their volumes result in 1.09 to 2.33 km^3. Fig. 3e shows an exception where no chaotic unit is observed and the HARS is truncated instead. However, in four out of five cases where MCS data cross the escarpments, the chaotic unit is observed.

4. Interpretation and discussion

We interpret the escarpments to be remnants of former submarine landslide events due to their morphology being limited in space and their basin-facing orientation transverse to the direction of the crest of the Lomonosov Ridge. The steep crescent-shaped headscarps open basinwards, therefore, leaving a pathway for sediments to escape. Subbottom data show semi-coherent parallel seafloor echoes indicative of a surficial sedimentary drape unit. Below this layer an acoustically chaotic subbottom reflection is typically observed in this area whereas outside the semi-coherent parallel stratification continues with depth. We interpret the chaotic unit to have been affected by the slide event or represent remnant slid material. A slightly basin-dipping high-amplitude reflection sequence (HARS) is imaged beneath the chaotic unit. Its partly eroded upper rim suggests that it has worked as glide plane. In our scenario, former potentially well-stratified sediments got instable within a restricted area. One part of the sediment moved basinwards along a glide plane whereas the other part got mixed up and remained on the glide plane. As a result of this process an escarpment with a crescent-shaped headwall was created. After this slide event, new sediments were deposited draping the new topography.

Table 1
Summary of the specific slide geometries, volumes, drape thickness and estimated ages.

Land-slide	Volume total/buried [km³]	Width [km]	Length [km]	Total height [m]	Headwall height [m]	Inclination			Thickness		Estimated age [Ma]
						Glide plane	Slope min/max	Headwall 1./3. quantile	Drape TWT in [ms]	Sediment[b] TWT in [ms]	
A	1.84/1.09	4.9	3.7	190	58	0.5°	4°/6°	6.8°/13.5°	~400	~550	13
B	3.60/2.33	5.7	4.1	413	172	~0°	5°/14°	8.3°/16.0°	~130	~550	4
C	7.58/x	10.2	8.2	851	x	x	3°/10°	3.4°/13.7°	x	x	x
D	2.64/1.52	5.1	4.7	282	207	0.9°[a]	1°/13°	8.2°/17.2°	~240	~580	7
E	2.23/1.66	4.5	3.7	125	70	0.6°	−1°/3°	5.2°/10.3°	~300	~680	9
F	3.03/x	8.4	5.9	222	147	–	3°/7°	6.1°/14.5°	–	–	x
G	0.09/x	2.1	1.7	231	112	–	7°/12°	11.0°/18.0°	–	–	x
H	1.96/x	5.9	4.8	374	129	–	3°/14°	10.2°/20.8°	–	–	x

x   no information available
–   no seismic data available to image this feature (see Fig. 1b, c)
[a]   Seismic profile located perpendicular to sliding direction
[b]   Above HARS.

Acoustically transparent, lens-shaped reflections within the drape indicate other generations of submarine mass wasting events with more recent and much smaller amounts of redeposited material. They did certainly not produce the escarpments studied here. Their further discussion, therefore, exceeds the scope of this paper and will be neglected hereafter. Fig. 3e shows, in contrast to all other submarine landslides with MCS data, a truncated HARS and no acoustically chaotic reflections which can be linked to the slide event. Therefore, this escarpment illustrates that also other types of slide processes occur on Lomonosov Ridge.

Submarine landslides are common worldwide (e.g. Canals et al., 2004; Mosher et al., 2010). Hereafter, we present a comparison between the volumes mobilized by submarine landslides in this study with selected slides distributed around the globe. They represent a vast variety of volumes mobilized by submarine landslide events. These volumes range from as small as 0.001 km³ (Finneidfjord, Canals et al., 2004) to as large as 3200 km³ (Storegga, Haflidason et al., 2005) (Fig. 4). The submarine landslides of the Lomonosov Ridge have failed sediment volumes of between 0.09 km³ and 7.58 km³. They are, therefore, small in a global context. As well, regarding their small volumina, we find their potential to cause tsunamis highly unlikely. Additionally, the large distance of the Lomonosov Ridge to the shelves and the vast shelves surrounding the Arctic Ocean would probably attenuate a runup of waves (Masson et al., 2006). The inclinations for headwall, glide plane and slope gradient, on the other hand, are consistent with inclinations reported by Canals et al. (2004): headwalls of up to 23°, glide planes below 1° and slope gradients between less than 2° but also up to 20°.

Such events also seem to be quite common on Lomonosov Ridge. Jokat (2005) reported indications for mass wasting events on AWI-98585-profile (location see Fig. 1a, c) and Pérez et al. (2020) found mass transport deposits in our research area. Kristoffersen et al. (2007) investigated seven fully imaged arc-shaped slide scars located on central Lomonosov Ridge between 87°15′ and 88°N (location see Fig. 1a). Similar to our new discoveries further towards the Siberian shelf, they are between 150 and 200 m high, 5 to 6 km wide and 7 to 9 km long, and occur on both flanks of Lomonosov Ridge.

Owing to the lack of deep scientific drilling holes within our research area, reliable age dating and information on the composition of the slid sediments is not possible. Instead, we use information gained from the Arctic Coring Expedition (ACEX) drill sites located more than 400 km to the north at the central Lomonosov Ridge. Backman et al. (2008) correlated the stratigraphic units from ACEX with seismic units of seismic reflection profile AWI-91090 (Jokat et al., 1992, 1995) crossing the drill site (Fig. 5c). Using this information Weigelt et al. (2014) correlated similarities in seismic reflection signal characteristics between the AWI-91090-profile and the 81°N-Transect (Jokat et al., 2013) across the Siberian end of Lomonosov

Ridge (Fig. 5a, c). Among these characteristics, a high amplitude reflection sequence (HARS) is a typical feature in the mentioned seismic data (AWI-91090, 81°N-Transect, this study; Fig. 5a–c). We apply their interpretation of a 18.2 Myr old age estimate for the upper boundary of the HARS (Weigelt et al., 2014) and use it as reference for our composition and age estimates.

The material above the HARS consists of silty clay to clayey silt (Backman et al., 2006) (Fig. 5). This is confirmed for the upper 7.5 m by gravity core and box-core samples within the study area (Stein, 2015, 2019). ACEX cores show that the HARS unit mainly consists of mud-bearing biosiliceous ooze (Backman et al., 2006) (Fig. 5). The traces of erosion at the interface between HARS and upper sediments in the escarpment area (Fig. 3c) indicate that the erosion was caused by the slide event. Therefore, the eroded material is most likely part of the failed material and, consequently, the failed material deposited on top of the eroded HARS is probably a mixture of silty clay to clayey silt and mud-bearing biosiliceous ooze.

Based on Weigelt et al. (2014) estimate of 18.2 Ma for the age of HARS, we suggest our submarine landslide events date from mid Miocene to mid Pliocene times. Sediments on top of the HARS accumulated with quite uniform sedimentation rates (Backman et al., 2008). We calculate average sedimentation rates of 26 and 29 m/Myr for the northern and southern research areas, respectively. Consequently, the landslides' drapes, with a thickness of 130 ms (~110 m) to 400 ms TWT (~340 m), needed between 4 and 13 Myr to accumulate.

The causes of specific submarine landslides are, in most cases, unknown. There are, however, several preconditioning factors that affect slope instability and common factors that act as triggers for slide events (Canals et al., 2004). Factors discussed here are the effects of free gas, sedimentation rates, bottom currents, sediment layering, glaciation and earthquakes.

Free intraformation gas and free gas can contribute to the initiation of submarine landslides by the generation of excess pore pressures (Best et al., 2003; Canals et al., 2004; Geissler et al., 2016). However, neither seismic reflection data nor core samples in our research area show indications for the presence of gas. Therefore, we exclude any gas releases as preconditioning or triggering factor for our landslides.

High sedimentation rates can cause sediment instability by generating excess pore pressures (Canals et al., 2004; Dugan and Sheahan, 2012; Masson et al., 2006). Sediment transport in the high Arctic is mainly controlled by the sea ice cover which hosts sediments from the adjacent continental margins and occasional turbidity currents (Dowdeswell et al., 1998; Nürnberg et al., 1994). This leads to a relatively low sediment input. Our sedimentation rates of only ≤29 m/Myr are likely to have been low enough to allow consolidation without overpressure (cf. Kristoffersen et al., 2007).
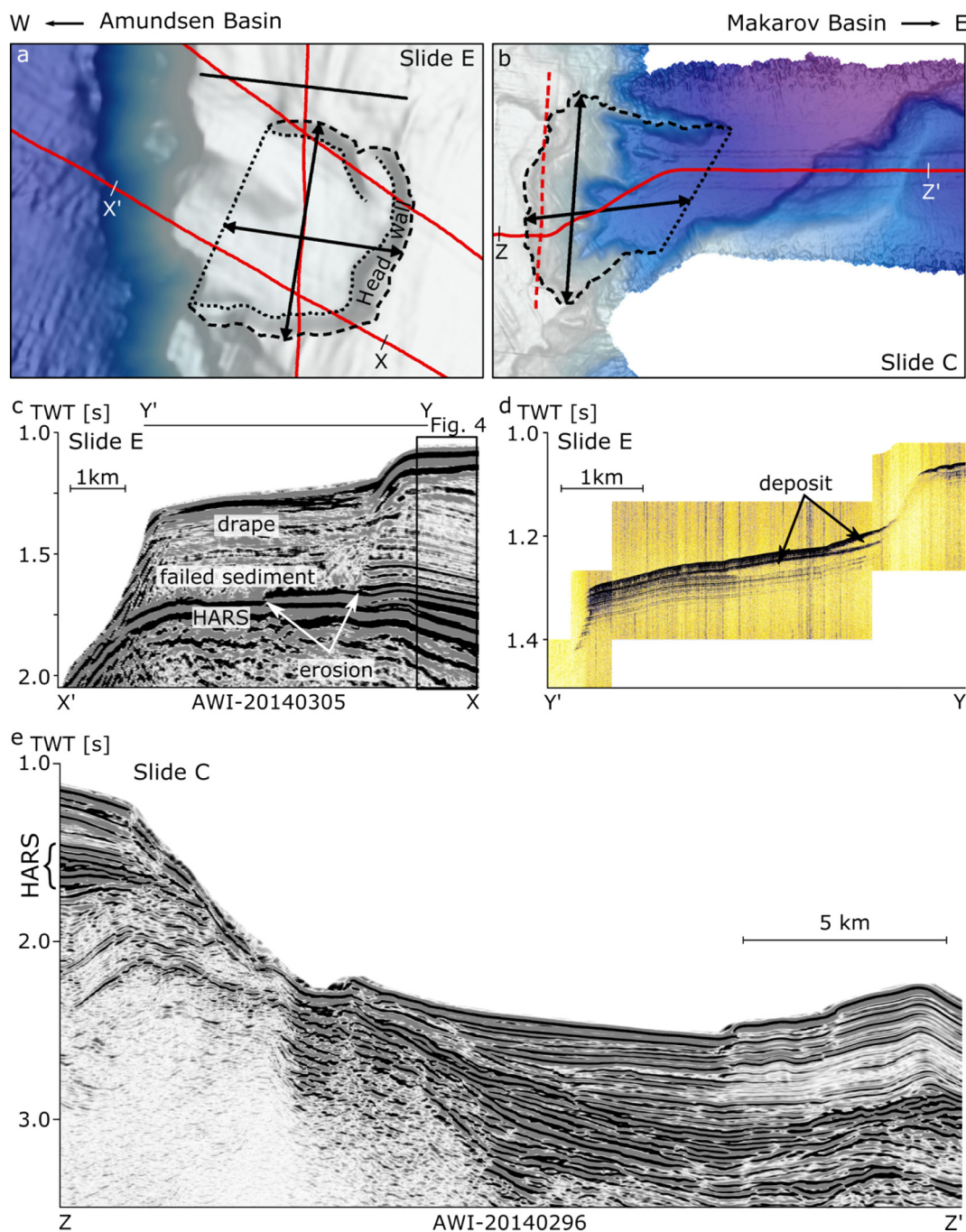
Fig. 3. Maps, seismic profiles and sediment echo sounder data for selected submarine landslides: (a) and (b) new swath bathymetry data of investigated landslides E and C, respectively (location see Fig. 1c). Headwalls are limited by their upper (dashed black lines) and lower (curved dotted black line) rims. Escarpment areas are limited by the top of headwall and a straight line (dotted black) connecting the endpoints of the top of headwall. Two-sided arrows: width and length of escarpment. For the remaining lines see Fig. 1. (c) and (e) seismic reflection profiles of landslides E and C, respectively. Note that in landslide E the chaotic, non-parallel reflections (failed sediments) overlain by quite well-stratified sediments (drape) and bounded at the bottom by a high-amplitude reflection sequence (HARS) that shows traces of erosion. (d) Sediment echo sounder section of landslide E showing acoustic transparent, lens-shaped features.

Bottom currents can directly excavate slide scar areas or contribute to slope instability by erosional undercutting and sediment redistribution (Kayen et al., 1989). Bottom currents flow in opposite directions on both sides of Lomonosov Ridge. Currents on the Amundsen Basin side flow from the Siberian end of the Lomonosov Ridge to Fram Strait (Jones, 2001; Rudels et al., 1994). Their mean speed velocities are 5 cm/s or lower. Mooring stations close to the study area measured speeds of eddy features of ~10 cm/s. This value decreases with increasing depth (Woodgate et al., 2001). Lower velocities are reported from the other side of Lomonosov Ridge, on the Makarov Basin side (Jones,

2001; Rudels et al., 1994; Woodgate et al., 2001). We assume bottom currents of <10 cm/s are not strong enough for sediment redistribution or slope undercutting. However, data from mooring stations measuring bottom current velocities close to Lomonosov Ridge are sparse and measurement periods are short (Aagaard, 1981; Rudels et al., 1994; Woodgate et al., 2001).

Unfavorable soil layering can be a preconditioning factor for submarine landslides (Vanneste et al., 2013). The HARS is indicative for a sedimentary layer with highly variable composition (Weigelt et al., 2020). During its development large changes in the deposition environment
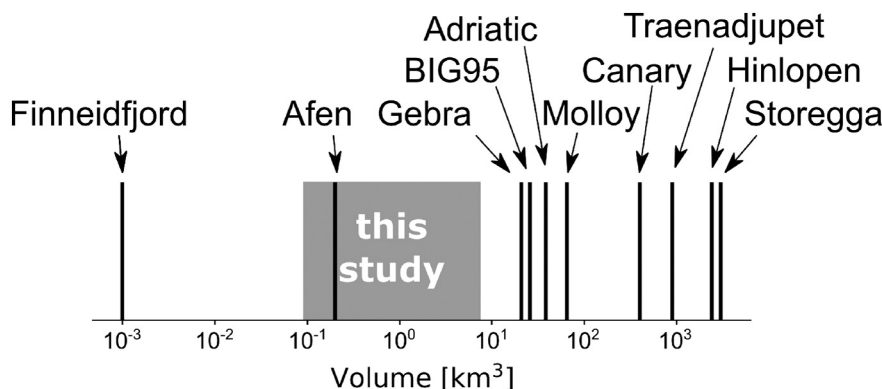
Fig. 4. Comparison of failed sediment volumes of submarine landslides: grey box: results of landslides discussed in this paper, black lines: global existing slides, source: Canals et al. (2004), Freire et al. (2014), Vanneste et al. (2006).

occurred due to the ongoing subsidence of Lomonosov Ridge below sea level to greater depths and the gradual opening of Fram Strait since early Oligocene leading, over time, to the modern ocean circulation system (e.g. Jakobsson et al., 2007; Jokat et al., 2016; Weigelt et al., 2020). Hemipelagic sedimentation prevailed before Miocene (Weigelt et al., 2020). Above this distinct sequence semi-coherent reflections with lower amplitude occur as a result of an established modern ocean circulation system since early Miocene (Jakobsson et al., 2007). Henceforward, pelagic sedimentation prevailed (Weigelt et al., 2020). MCS data show that the interface between the HARS and the low-amplitude sequence above repeatedly acted as glide plane. Therefore, we propose that the rapid transformation from predominantly hemipelagic to pelagic sedimentation was a preconditioning factor for the slide events.

Another scenario, specific to the polar regions, is sea floor erosion by iceberg keels or grounded ice during phases of glacial expansion and retreat. Other glaciated margins were to a large extend massively overprinted by numerous glacial events (e.g. East Greenland (Arndt et al., 2017), Chukchi Margin (Polyak et al., 2007)). However, on most of these margins only structures of the Last Glacial Maximum caused by glaciers or ice streams can be observed. This is different to Lomonosov Ridge, which never hosted any ice streams or glaciers but was affected by large grounded ice bergs. Stein et al. (2016) and Jakobsson et al. (2016) presented such evidence in form of glacial lineations indicating events of grounding ice within our research area. Stein et al. (2016) dated the lineations to "Quaternary glaciations, for example, during Marine Isotope Stage 6" (140 ka, Jakobsson et al., 2010). Numerous studies suggest however that the modern pattern of Northern Hemisphere glacial/interglacial cycles initiated well after the slide events depicted here (e.g. Brigham-Grette et al., 2013; Dipre et al.,

2018; Moran et al., 2006). Consequently, it is highly unlikely that the landslides were triggered by grounded ice or iceberg keels.

Earthquakes are often considered as triggers for submarine slide events (Biscontin et al., 2004; Canals et al., 2004; Masson et al., 2006). Within the last 50 years very few earthquakes (3) were detected on Lomonosov Ridge (International Seismological Centre, 2020). However, the current distribution of seismometers of the International Seismological Centre (ISC) lacks seismological instruments on or close to the ridge (Fig. 1a) (International Seismological Centre, 2020). This suggests that the Lomonosov Ridge is likely to be affected by a larger number of lower magnitude earthquakes. The geological history of Lomonosov Ridge includes its separation from the Barents–Kara Sea ~56 Ma (Jokat et al., 1995; Karasik, 1968; Vogt et al., 1979) followed by a continuous subsidence below sea level ~6 Myr later (Jokat et al., 1995). Scientific drilling on ACEX-site on central Lomonosov Ridge revealed that the ridge continued its subsidence below sea level through Miocene and thereafter until it reached its present depth (Moore, 2006; Piskarev et al., 2019). Earthquakes have likely co-occurred during the entire Cenozoic subsidence history of Lomonosov Ridge until present. It can therefore not be excluded that different earthquakes of different magnitudes could have triggered failure depending on the actual degree of sediment instability.

5. Conclusion

Systematic swath bathymetry on the Siberian part of Lomonosov Ridge (81°–84°N, 140°–146°E) revealed twelve previously unknown submarine landslides from both flanks of the Lomonosov Ridge. A detailed study of eight of the landslides revealed that they are buried by
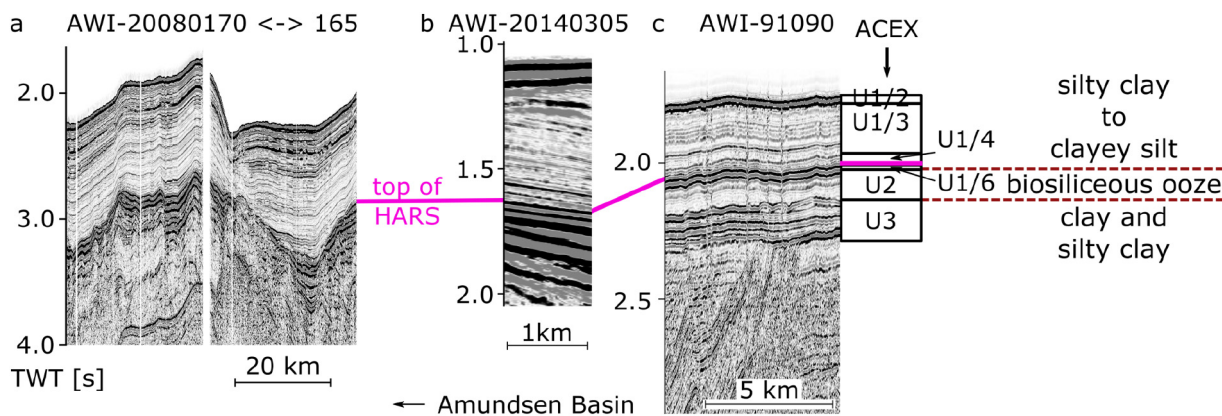

Fig. 5. Compilation of seismic lines (a) AWI-20080170 to AWI-20080165 on 81°N-Transect (Jokat et al., 2013; Weigelt et al., 2014) (location see Fig. 1a, yellow line segment), (b) AWI-20140305 close to landslide E (location see Fig. 3a, c), and (c) AWI-91090 (Jokat et al., 1992, 1995) (location see Fig. 1a) tied to ACEX lithology (Backman et al., 2006). Correlations of the top of the high-amplitude sequence (HARS) (pink) are shown between seismic profiles and the Arctic Coring Expedition (ACEX). Figure modified after Weigelt et al. (2014).

~110–340 m of post-slide sediments. These landslides have spatial extents of several kilometers (2.1–10.2 km wide, 1.7–8.2 km long, 125–851 m high) and headwall heights of 58–207 m. Volumes of failed slide material range from 0.09 to 7.58 km³ and, in most of the investigated landslides, a less than 1° basin dipping high-amplitude reflection sequence (HARS) - visible in seismic profiles - repeatedly functioned as glide plane.

Compared with worldwide existing submarine landslides, the investigated landslides are small. Previous discoveries of similar events on central Lomonosov Ridge imply, however, that landslides of these dimensions are common on the ridge. Inclinations, on the other hand, namely of headwall, glide plane and slope gradient, are within global typical value ranges for submarine landslides.

The failed slide material quite likely consists of silty clay to clayey silt possibly mixed with biosiliceous ooze. The mapped slide events most likely occurred between mid Pliocene and mid Miocene. We propose that the rapid transformation from predominantly hemipelagic to pelagic sedimentation as indicated by the sharp transition from the HARS to a low-amplitude sequence in MCS data, preconditioned the submarine landslides. We further suggest earthquakes have triggered the submarine landslides, as they are likely to have occurred during the continuous subsidence of Lomonosov Ridge since its separation from the Siberian shelves.

Data availability

The seismic data set is archived under https://doi.pangaea.de/10.1594/PANGAEA.919774, bathymetry and Parasound data can be found at https://doi.pangaea.de/10.1594/PANGAEA.857857 and https://doi.pangaea.de/10.1594/PANGAEA.839763, respectively.

Declaration of competing interest

The authors declare that they have no known competing financial interests or personal relationships that could have appeared to influence the work reported in this paper.

Acknowledgements

References

Aagaard, K., 1981. On the deep circulation in the Arctic Ocean, Deep Sea Research Part A. Oceanographic Research Papers 28 (3), 251–268. https://doi.org/10.1016/0198-0149(81)90066-2.

Arndt, J.E., Jokat, W., Dorschel, B., 2017. The last glaciation and deglaciation of the Northeast Greenland continental shelf revealed by hydro-acoustic data. Quat. Sci. Rev. 160, 45–56. https://doi.org/10.1016/j.quascirev.2017.01.018.

Backman, J., K. Moran, D. B. McInroy, L. A. Mayer, and a. t. E. Scientists (2006), Sites M0001–M0004, in Proceedings of the Integrated Ocean Drilling Program (IODP), edited, (Integrated Ocean Drilling Program Management International, Inc.), Edinburgh, doi:https://doi.org/10.2204/iodp.proc.302.104.2006.

Backman, J., et al., 2008. Age model and core-seismic integration for the Cenozoic Arctic Coring Expedition sediments from the Lomonosov Ridge. Paleoceanography 23 (1). https://doi.org/10.1029/2007PA001476.

Best, A. I., C. R. I. Clayton, O. Longva, and M. Szuman (2003), The role of free gas in the activation of submarine slides in Finneidfjord, in Submarine Mass Movements and their Consequences: 1st International Symposium, edited by J. Locat, J. Mienert and L. Boisvert, pp. 491–498, Springer Netherlands, Dordrecht, doi:https://doi.org/10.1007/978-94-010-0093-2_54.

Biscontin, G., Pestana, JM., Nadim, F., 2004. Seismic triggering of submarine slides in soft cohesive soil deposits. Mar. Geol. 203 (3–4), 341–354. https://doi.org/10.1016/S0025-3227(03)00314-1.

Boggild, K., Mosher, D.C., Travaglini, P., Gebhardt, C., Mayer, L., 2020. Mass wasting on Alpha Ridge in the Arctic Ocean: new insights from multibeam bathymetry and sub-bottom profiler data. Geol. Soc. Lond., Spec. Publ. 500 (1), 323. https://doi.org/10.1144/SP500-2019-196.

Brigham-Grette, J., et al., 2013. Pliocene warmth, polar amplification, and stepped pleistocene cooling recorded in NE Arctic Russia. Science 340 (6139), 1421–1427. https://doi.org/10.1126/science.1233137.

Bryn, P., A. Solheim, K. Berg, R. Lien, C. F. Forsberg, H. Haflidason, D. Ottesen, and L. Rise (2003), The Storegga slide complex; repeated large scale sliding in response to climatic cyclicity, in Submarine Mass Movements and Their Consequences: 1st International Symposium, edited by J. Locat, J. Mienert and L. Boisvert, pp. 215–222, Springer Netherlands, Dordrecht, doi:https://doi.org/10.1007/978-94-010-0093-2_24.

Bugge, T., Befring, S., Belderson, R.H., Eidvin, T., Jansen, E., Kenyon, N.H., Holtedahl, H., Sejrup, H.P., 1987. A giant three-stage submarine slide off Norway. Geo-Mar. Lett. 7 (4), 191–198. https://doi.org/10.1007/BF02242771.

Bugge, T., R. H. Belderson, and N. H. Kenyon (1988), The Storegga slide, Philosophical Transactions - Royal Society, Series A, 325(1586), 358-ca.390.

Canals, M., et al., 2004. Slope failure dynamics and impacts from seafloor and shallow subseafloor geophysical data: case studies from the COSTA project. Mar. Geol. 213 (1–4), 9–72. https://doi.org/10.1016/j.margeo.2004.10.001.

Clare, M., et al. (2019), A consistent global approach for the morphometric characterization of subaqueous landslides, in Geological Society Special Publication, edited, pp. 455–477, doi:https://doi.org/10.1144/SP477.15.

Dipre, G.R., Polyak, L., Kuznetsov, A.B., Oti, E.A., Ortiz, J.D., Brachfeld, S.A., Xuan, C., Lazar, K. B., Cook, A.E., 2018. Plio-Pleistocene sedimentary record from the Northwind Ridge: new insights into paleoclimatic evolution of the western Arctic Ocean for the last 5 Ma. arktos 4 (1), 24. https://doi.org/10.1007/s41063-018-0054-y.

Dowdeswell, J.A., Elverhfi, A., Spielhagen, R., 1998. Glacimarine sedimentary processes and facies on the polar north Atlantic margins. Quat. Sci. Rev. 17 (1), 243–272. https://doi.org/10.1016/S0277-3791(97)00071-1.

Dugan, B., Sheahan, T.C., 2012. Offshore sediment overpressures of passive margins: mechanisms, measurement, and models. Rev. Geophys. 50 (3). https://doi.org/10.1029/2011RG000379.

Freire, F., Gyllencreutz, R., Jafri, R.U., Jakobsson, M., 2014. Acoustic evidence of a submarine slide in the deepest part of the Arctic, the Molloy Hole. Geo-Mar. Lett. 34 (4), 315–325. https://doi.org/10.1007/s00367-014-0371-5.

Geissler, W.H., Gebhardt, A.C., Gross, F., Wollenburg, J., Jensen, L., Schmidt-Aursch, M.C., Krastel, S., Elger, J., Osti, G., 2016. Arctic megaslide at presumed rest. Sci. Rep. 6 (1), 38529. https://doi.org/10.1038/srep38529.

Haflidason, H., Sejrup, H.P., Nygård, A., Mienert, J., Bryn, P., Lien, R., Forsberg, C.F., Berg, K., Masson, D., 2004. The Storegga slide: architecture, geometry and slide development. Mar. Geol. 213 (1–4), 201–234. https://doi.org/10.1016/j.margeo.2004.10.007.

Haflidason, H., Lien, R., Sejrup, H.P., Forsberg, C.F., Bryn, P., 2005. The dating and morphometry of the Storegga slide. Mar. Pet. Geol. 22(1-2 SPEC. ISS.), 123-136. https://doi.org/10.1016/j.marpetgeo.2004.10.008.

International Seismological Centre (2020), On-line Bulletin, doi:https://doi.org/10.31905/D808B830, accessed: 01.07.2020.

Jakobsson, M., et al., 2007. The early Miocene onset of a ventilated circulation regime in the Arctic Ocean. Nature 447. https://doi.org/10.1038/nature05924.

Jakobsson, M., et al., 2010. An Arctic Ocean ice shelf during MIS 6 constrained by new geophysical and geological data. Quat. Sci. Rev. 29 (25–26), 3505–3517. https://doi.org/10.1016/j.quascirev.2010.03.015.

Jakobsson, M., et al., 2012. The International Bathymetric Chart of the Arctic Ocean (IBCAO) version 3.0. Geophys. Res. Lett. 39 (12). https://doi.org/10.1029/2012gl052219.

Jakobsson, M., et al., 2016. Evidence for an ice shelf covering the central Arctic Ocean during the penultimate glaciation. Nat. Commun. 7. https://doi.org/10.1038/ncomms10365.

Jokat, W., 2005. The sedimentary structure of the Lomonosov Ridge between 88°N and 80°N. Geophys. J. Int. 163 (2), 698–726. https://doi.org/10.1111/j.1365-246X.2005.02786.x.

Jokat, W., Uenzelmann-Neben, G., Kristoffersen, Y., Rasmussen, T.M., 1992. Lomonosov Ridge - a double-sided continental margin. Geology 20 (10), 887–890. https://doi.org/10.1130/0091-7613(1992)020<0887:LRADSC>2.3.CO;2.

Jokat, W., Weigelt, E., Kristoffersen, Y., Rasmussen, T., Schöne, T., 1995. New insights into the evolution of the Lomonosov Ridge and the Eurasian Basin. Geophys. J. Int. 122 (2), 378–392. https://doi.org/10.1111/j.1365-246X.1995.tb00532.x.

Jokat, W., Ickrath, M., O'Connor, J., 2013. Seismic transect across the Lomonosov and Mendeleev Ridges: Constraints on the geological evolution of the Amerasia Basin, Arctic Ocean, Geophys. Res. Lett. 40. https://doi.org/10.1002/grl.50975.

Jokat, W., Lehmann, P., Damaske, D., Nelson, J. Bradley, 2016. Magnetic signature of North-East Greenland, the Morris Jesup Rise, the Yermak Plateau, the central Fram Strait: constraints for the rift/drift history between Greenland and Svalbard since the Eocene. Tectonophysics 691, 98–109. https://doi.org/10.1016/j.tecto.2015.12.002.

Jones, E.P., 2001. Circulation in the Arctic Ocean. Polar Res. 20 (2), 139–146. https://doi.org/10.1111/j.1751-8369.2001.tb00049.x.

Karasik, A. M. (1968), Magnetic anomalies of the Gakkel Ridge and origin of the Eurasia Subbasin of the Arctic Ocean, Geophys. Methods Prospect. Arctic, 5(5), 8–19.

Kayen, R.E., Schwab, W.C., Lee, H.J., Torresan, M.E., Hein, J.R., Quinterno, P.J., Levin, L.A., 1989. Morphology of sea-floor landslides on Horizon Guyot: application of steady-state geotechnical analysis. Deep Sea Research Part A, Oceanographic Research Papers 36 (12), 1817–1839. https://doi.org/10.1016/0198-0149(89)90114-3.

Kristoffersen, Y., Coakley, B.J., Hall, J.K., Edwards, M., 2007. Mass wasting on the submarine Lomonosov Ridge, central Arctic Ocean. Mar. Geol. 243 (1), 132–142. https://doi.org/10.1016/j.margeo.2007.04.012.

Kristoffersen, Y., Hall, J.K., Hunkins, K., Ardai, J., Coakley, B.J., Hopper, J.R., Seismic, T. Healy, 2008. Extensive local seabed disturbance, erosion and mass wasting on Alpha Ridge, Central Arctic Ocean: possible evidence for an extra-terrestrial impact?, Norw. J. Geol. 88 (4), 313–320.

Laberg, J.S., Kawamura, K., Amundsen, H., Baeten, N., Forwick, M., Rydningen, T.A., Vorren, T.O., 2014. A submarine landslide complex affecting the Jan Mayen Ridge, Norwegian-Greenland Sea: slide-scar morphology and processes of sediment evacuation. Geo-Mar. Lett. 34 (1), 51–58. https://doi.org/10.1007/s00367-013-0345-z.

Masson, D.G., Harbitz, C.B., Wynn, R.B., Pedersen, G., Løvholt, F., 2006. Submarine landslides: processes, triggers and hazard prediction. Philos. Trans. R. Soc. A Math. Phys. Eng. Sci. 364 (1845), 2009–2039. https://doi.org/10.1098/rsta.2006.1810.

Moore, T.C., 2006. Sedimentation and subsidence history of the Lomonosov Ridge. Proc. IODP 1–7.

Moran, K., et al., 2006. The Cenozoic palaeoenvironment of the Arctic Ocean. Nature 441 (7093), 601–605. https://doi.org/10.1038/nature04800.

Mosher, D.C., Shipp, R.C., Moscardelli, L., Chaytor, J.D., Baxter, C.D.P., Lee, H.J., Urgeles, R., 2010. Submarine Mass Movements and Their Consequences. Springer, Dordrecht https://doi.org/10.1007/978-90-481-3071-9.

Mosher, D. C., J. Shimeld, D. Hutchinson, N. Lebedeva-Ivanova, and C. B. Chapman (2012), Submarine Landslides in Arctic Sedimentation: Canada Basin, Paper Presented at Submarine Mass Movements and their Consequences, Springer Netherlands, Dordrecht, 2012//.

Nürnberg, D., Wollenburg, I., Dethleff, D., Eicken, H., Kassens, H., Letzig, T., Reimnitz, E., Thiede, J., 1994. Sediments in Arctic sea ice: Implications for entrainment, transport and release. Mar. Geol. 119 (3), 185–214. https://doi.org/10.1016/0025-3227(94)90181-3.

Pérez, L.F., Jakobsson, M., Funck, T., Andresen, K.J., Nielsen, T., O'Regan, M., Mørk, F., 2020. Late Quaternary sedimentary processes in the central Arctic Ocean inferred from geophysical mapping. Geomorphology 369, 107309. https://doi.org/10.1016/j.geomorph.2020.107309.

Piskarev, A.L., Butsenko, V.V., Chernykh, A.A., Ivanov, M.V., Kaminsky, V.D., Poselov, V.A., Savin, V.A., 2019. Lomonosov Ridge. In: Piskarev, A., Poselov, V., Kaminsky, V. (Eds.), Geologic Structures of the Arctic Basin. Springer International Publishing, Cham, pp. 157–185 https://doi.org/10.1007/978-3-319-77742-9_4.

Polyak, L, Darby, D.A., Bischof, J.F., Jakobsson, M., 2007. Stratigraphic constraints on late Pleistocene glacial erosion and deglaciation of the Chukchi margin. Arctic Ocean, Quaternary Research 67 (2), 234–245. https://doi.org/10.1016/j.yqres.2006.08.001.

Rudels, B., Jones, E.P., Anderson, L.G., Kattner, G., 1994. On the intermediate depth waters of the Arctic Ocean. The Polar Oceans and Their Role in Shaping the Global Environment 85, 33–46.

Safronova, P.A., Laberg, J.S., Andreassen, K., Shlykova, V., Vorren, T.O., Chernikov, S., 2017. Late Pliocene–early Pleistocene deep-sea basin sedimentation at high-latitudes: mega-scale submarine slides of the north-western Barents Sea margin prior to the shelf-edge glaciations. Basin Res. 29, 537–555. https://doi.org/10.1111/bre.12161.

Stein, R. (2015), The Expedition PS87 of the Research Vessel POLARSTERN to the Arctic Ocean in 2014, edited, Alfred Wegener Institute for Polar and Marine Research, Bremerhaven, doi:https://doi.org/10.2312/BzPM_0688_2015.

Stein, R. (2019), The Expedition PS115/2 of the Research Vessel POLARSTERN to the Arctic Ocean in 2018, edited, Alfred Wegener Institute for Polar and Marine Research, Bremerhaven, doi:https://doi.org/10.2312/BzPM_0728_2019.

Stein, R., et al., 2016. Evidence for ice-free summers in the late Miocene central Arctic Ocean. Nat. Commun. 7 (1), 11148. https://doi.org/10.1038/ncomms11148.

Vanneste, M., Mienert, J., Bünz, S., 2006. The Hinlopen Slide: a giant, submarine slope failure on the northern Svalbard margin, Arctic Ocean. Earth Planet. Sci. Lett. 245 (1–2), 373–388. https://doi.org/10.1016/j.epsl.2006.02.045.

Vanneste, M., C. Forsberg, S. Glimsdal, C. Harbitz, D. Issler, T. Kvalstad, F. Løvholt, and F. Nadim (2013), Submarine landslides and their consequences: what do we know, what can we do?, (Keynote Presentation and Paper), 2nd World Landslide Forum, Rome, Italy, 5, doi:https://doi.org/10.1007/978-3-642-31427-8-1.

Vogt, P. R., P. T. Taylor, L. C. Kovacs, and G. L. Johnson (1979), Detailed aeromagnetic investigation of the Arctic Basin, Journal of Geophysical Research: Solid Earth, 84(B3), 1071–1089, doi:https://doi.org/10.1029/JB084iB03p01071.

Vogt, P.R., Crane, K., Sundvor, E., Hjelstuen, B.O., Gardner, J., Bowles, F., Cherkashev, G., 1999. Ground-Truthing 11- to 12-kHz side-scan sonar imagery in the Norwegian–Greenland Sea: Part II: probable diapirs on the Bear Island fan slide valley margins and the Vøring Plateau. Geo-Mar. Lett. 19 (1), 111–130. https://doi.org/10.1007/s003670050099.

Weigelt, E., Jokat, W., Franke, D., 2014. Seismostratigraphy of the Siberian sector of the Arctic Ocean and adjacent Laptev Sea Shelf. J. Geophys. Res. Solid Earth 119. https://doi.org/10.1002/2013JB010727.

Weigelt, E., Jokat, W., Eisermann, H., 2020. Deposition history and Paleo-current activity on the Southeastern Lomonosov Ridge and its Eurasian Flank based on seismic data. Geochemistry Geophysics Geosystems 21, e2020GC009133. https://doi.org/10.1029/2020GC009133.

Winkelmann, D., Jokat, W., Niessen, F., Stein, R., Winkler, 2006. Age and extent of the Yermak Slide north of Spitsbergen. Arctic Ocean, Geochemistry, Geophysics, Geosystems 7 (6). https://doi.org/10.1029/2005GC001130.

Woodgate, R.A., Aagaard, K., Muench, R.D., Gunn, J., Björk, G., Rudels, B., Roach, A.T., Schauer, U., 2001. The Arctic Ocean boundary current along the Eurasian slope and the adjacent Lomonosov ridge: water mass properties, transports and transformations from moored instruments. Deep-Sea Research Part I: Oceanographic Research Papers 48 (8), 1757–1792. https://doi.org/10.1016/S0967-0637(00)00091-1.

Zoraster, S., 2003. A surface modeling algorithm designed for speed and ease of use with all petroleum industry data. Comput. Geosci. 29 (9), 1175–1182. https://doi.org/10.1016/s0098-3004(03)00139-0.